Zfp521 controls bone mass by HDAC3-dependent attenuation of Runx2 activity

Eric Hesse,[1,2] Hiroaki Saito,[1,2] Riku Kiviranta,[1,2] Diego Correa,[1,2] Kei Yamana,[1,2,3] Lynn Neff,[1,2] Daniel Toben,[4,5] Georg Duda,[4,5] Azeddine Atfi,[1,2] Valérie Geoffroy,[6] William C. Horne,[1,2] and Roland Baron[1,2]

[1]Department of Medicine, Harvard Medical School, and [2]Department of Oral Medicine, Infection, and Immunity, Harvard School of Dental Medicine, Harvard University, Boston, MA 02115
[3]Teijin Pharma Limited, Teijin Institute for Biomedical Research, Hino, Tokyo 191-8512, Japan
[4]Julius Wolff Institute and Center for Musculoskeletal Surgery and [5]Berlin-Brandenburg Center for Regenerative Therapies, Charité University of Medicine Berlin, D-13353 Berlin, Germany
[6]Institut National de la Santé et de la Recherche Medicale U606, Université Paris Diderot-Paris 7, Hôpital Lariboisière, 75475 Paris, Cedex 10, France

Runx2 is indispensable for osteoblast lineage commitment and early differentiation but also blocks osteoblast maturation, thereby causing bone loss in Runx2 transgenic mice. Zinc finger protein 521 (Zfp521) antagonizes Runx2 in vivo. Eliminating one *Zfp521* allele mitigates the cleidocranial dysplasia–like phenotype of newborn *Runx2*$^{+/-}$ mice, whereas overexpressing Zfp521 exacerbates it. Overexpressing Zfp521 also reverses the severe osteopenia of adult Runx2 transgenic mice. Zfp521 binds to both Runx2 and histone deacetylase 3 (HDAC3), promotes their association, and antagonizes Runx2 transcriptional activity in an HDAC3-dependent manner. Mutating the Zfp521 zinc finger domains 6 and 26 reduces the binding of Zfp521 to Runx2 and inhibition of Runx2 activity. These data provide evidence that Zfp521 antagonizes Runx2 in vivo and thereby regulates two stages of osteoblast development, early during mesenchymal cell lineage commitment and later during osteoblast maturation. Thus, the balance and molecular interplay between Zfp521 and Runx2 contribute to the control of osteoblast differentiation, skeletal development, and bone homeostasis.

Introduction

Development and life-long maintenance of the bones comprising the mammalian skeleton is evolutionarily conserved and tightly regulated (Karsenty et al., 2009). The modeling of skeletal elements during development, largely starting from cartilaginous templates, requires the coordinated actions of matrix-resorbing osteoclasts and matrix-producing osteoblasts. The mature skeleton is then constantly remodeled by the coupled activities of these two cell types. With age, bone formation decreases below the level required to compensate for the often-increased bone resorption, leading to osteoporosis with its associated fractures. It is therefore of great clinical importance to identify and characterize in depth the molecular mechanisms that regulate osteoblast differentiation, osteoblast function, and, hence, bone formation.

Osteoblasts differentiate from mesenchymal precursor cells, which can also give rise to adipocytes, chondrocytes, and myoblasts (Harada and Rodan, 2003). Downstream of key osteogenic signaling pathways, such as bone morphogenetic protein/Smad or canonical Wnt, lineage-specific transcription factors regulate specific steps in the progressive transition from early mesenchymal cells to the fully differentiated bone matrix–producing osteoblasts (Karsenty et al., 2009).

Runx2, a Runt domain transcription factor, is essential for the commitment of early mesenchymal cells to the osteoblast lineage (Ducy et al., 1997; Karsenty et al., 2009). In addition, Runx2 controls the differentiation and function of the osteoblast in concert with other factors such as Osterix (Osx) by regulating the expression of many osteoblast-related genes

Correspondence to Roland Baron: roland_baron@hsdm.harvard.edu

Abbreviations used in this paper: ALP, alkaline phosphatase; BV/TV, bone volume per tissue volume; CCD, cleidocranial dysplasia; CFU-F, colony-forming unit–fibroblast; CFU-OB, colony-forming unit–osteoblast; Dmp-1, Dentin matrix protein 1; HDAC, histone deacetylase; Ko, knockout; mRIPA, modified radioimmunoprecipitation assay; NuRD, nucleosome remodeling and HDAC; Opg, Osteoprotegerin; OSE2, osteoblast-specific element 2; Osx, Osterix; Rankl, receptor activator for nuclear factor κB ligand; ROS, rat osteosarcoma cell line; shRNA, short hairpin RNA; TSA, trichostatin A; Wt, wild type; ZF, zinc finger; Zfp521, zinc finger protein 521.

The Rockefeller University Press $30.00
J. Cell Biol. Vol. 191 No. 7 1271–1283
www.jcb.org/cgi/doi/10.1083/jcb.201009107

(e.g., *collagen I*, *osteocalcin*, *MMP13*, and *osteopontin*; Nakashima et al., 2002; Stein et al., 2004), including the *Runx2* gene itself (Drissi et al., 2000).

Knockout (Ko) studies have demonstrated that the skeletons of *Runx2*$^{-/-}$ mice are blocked at the cartilage stage without mineralized bones because of a lack of osteoblast differentiation, illustrating the requirement of Runx2 at early stages of osteoblast differentiation. Because of the failure of the skeleton to mineralize, *Runx2*$^{-/-}$ animals suffer from respiratory insufficiency and die shortly after birth (Komori et al., 1997; Otto et al., 1997). The biological and clinical relevance of Runx2 was further demonstrated by the identification of mutations in the *Runx2* gene locus in humans with autosomal dominant cleidocranial dysplasia (CCD; Mundlos et al., 1997). Because of the reduced *Runx2* gene dose caused by these mutations, affected patients develop clavicle hypoplasia and craniofacial abnormalities, a phenotype that is largely recapitulated in mice heterozygous for *Runx2* (Mundlos et al., 1997; Otto et al., 1997, 2002).

In sharp contrast to the positive effect of Runx2 on osteoblast lineage commitment and early osteoblast differentiation, it has been hypothesized that Runx2 may inhibit osteoblast maturation because overexpression of Runx2 targeted to differentiating osteoblasts leads to osteopenia and ultimately sporadic fractures of the hind-limb long bones in adult mice (Liu et al., 2001; Geoffroy et al., 2002). These findings suggest that the effect of Runx2 activity on osteoblast function and bone mass may be differentiation stage dependent. Thus, as much as Runx2 is necessary for the commitment and early differentiation of osteoblast precursors, the attenuation of its activity at later stages is likely equally important for the final maturation and function of osteoblasts (Lian and Stein, 2003). Negative regulation of Runx2 activity can occur at the transcriptional and posttranslational level and is exerted by a complex interplay of a variety of factors, including transcriptional repressors (de Frutos et al., 2009), homeodomain proteins (Hassan et al., 2004, 2009), and histone deacetylases (HDAC; Westendorf et al., 2002; Schroeder et al., 2004; Kang et al., 2005; Jensen et al., 2008, 2009).

We recently reported zinc finger protein 521 (Zfp521) as a transcriptional repressor that attenuates Runx2 activity in vitro (Wu et al., 2009). In the present study, we establish the repressive role of Zfp521 on Runx2 and early osteoblast differentiation in vivo by genetic experiments, demonstrating that removing one allele of *Zfp521* partially rescues the CCD phenotype of *Runx2*$^{+/-}$ mice, whereas overexpressing Zfp521 enhances it. We then identify the molecular mechanism underlying the repression of Runx2 transcriptional activity by Zfp521 and demonstrate that Zfp521 also interacts with the corepressor HDAC3, stabilizing the interaction between Runx2 and HDAC3. Finally, we test the hypothesis that Runx2 indeed exerts opposite functions at early and late stages of osteoblast differentiation and find that overexpressed Zfp521 prevents the onset of osteopenia and sporadic long bone fractures in Runx2 transgenic mice. Together, these findings provide strong in vivo evidence for both the physiological repression of Runx2 by Zfp521 and the dual role of Runx2, favoring osteoblast commitment and early differentiation but opposing osteoblast maturation.

Results

Zfp521 modulates the CCD phenotype in *Runx2*$^{+/-}$ mice

Runx2$^{+/-}$ mice display features of the human heritable disease CCD, including hypoplastic clavicles, a hypoplastic hyoid bone with a delay in mineralization, and open fontanelles (Mundlos et al., 1997; Otto et al., 1997). Because this phenotype is a consequence of the reduced *Runx2* gene dose, we hypothesized that if Zfp521 indeed antagonizes Runx2 in vivo, removing one allele of *Zfp521* would lessen the CCD phenotype, whereas overexpressing Zfp521 would enhance it. To test this hypothesis under physiological conditions, we used the compound heterozygous strategy. First we generated mice with a heterozygous germline deletion of *Zfp521* (*Zfp521*$^{+/-}$) and crossed these animals with *Runx2*$^{+/-}$ mice to generate *Zfp521*$^{+/-}$*;Runx2*$^{+/-}$ double heterozygous mice, *Zfp521*$^{+/-}$ and *Runx2*$^{+/-}$ single heterozygous mice, and *wild-type* (*Wt*) littermates. Analysis of postnatal day (P) 0 skeletal preparations revealed that the length of both the clavicle and the mineralized midportion of the hyoid bone was significantly increased in *Zfp521*$^{+/-}$ mice compared with *Wt* littermates. Furthermore, the hypoplasia of the clavicle and the delayed mineralization of the midportion of the hyoid bone of the *Runx2*$^{+/-}$ mice were partially normalized in the *Zfp521*$^{+/-}$*; Runx2*$^{+/-}$ mice (Fig. 1, A and B), suggesting that Zfp521 indeed acts to oppose Runx2-induced osteoblast differentiation and bone mineralization under physiological conditions in vivo.

We sought to further investigate the Zfp521-mediated antagonism of Runx2 activity by generating bitransgenic mice in which overexpression of Zfp521 was regulated by the enolase 2 (ENO2) promoter (*ENO2-tTA;TetOp-Zfp521* mice, hereafter referred to as *Zfp521*^{Tg} mice). We successfully used this bitransgenic system in earlier osteoblast-related work (Sabatakos et al., 2000, 2008; Rowe et al., 2009) and selected it for this study because the ENO2 promoter is active in both early osteoblasts (Fig. S1 A) and in more mature osteoblasts in the long bones of adult mice (Fig. S4 A). In addition, the ENO2 promoter is not regulated by Runx2 (unpublished data), unlike many of the classical promoters used to control overexpression in subsets of osteoblasts such as Osx, Collagen I, or Osteocalcin.

In brief, *Zfp521*^{Tg} mice were crossed with *Runx2*$^{+/-}$ mice to generate *Zfp521*^{Tg}*;Runx2*$^{+/-}$ compound mice, *Zfp521*^{Tg} mice, *Runx2*$^{+/-}$ mice, and *Wt* littermates. Analysis of skeletal preparations revealed that at P2, the clavicle and hyoid bone of the *Zfp521*^{Tg} mice were hypoplastic and intermediate between *Wt* and *Runx2*$^{+/-}$ mice (Fig. 1, C and D). More importantly, the CCD phenotype of the *Runx2*$^{+/-}$ mice was significantly enhanced in the *Zfp521*^{Tg}*;Runx2*$^{+/-}$ compound mice, in which the rudimentary clavicle was greatly reduced in length and thickness (Fig. 1 C), and the midportion of the hypoplastic hyoid bone lacked any mineralization at P2 (Fig. 1 D). The *Runx2*$^{+/-}$ mice demonstrated a clearly defined nonmineralized area between the anterior and posterior fontanelles at 25 d of age, which was strikingly larger in the *Zfp521*^{Tg}*;Runx2*$^{+/-}$ mice (Fig. 1 E). These data demonstrate that Zfp521 antagonizes the pro-osteogenic function of Runx2 at early stages of osteoblast commitment and differentiation in vivo.

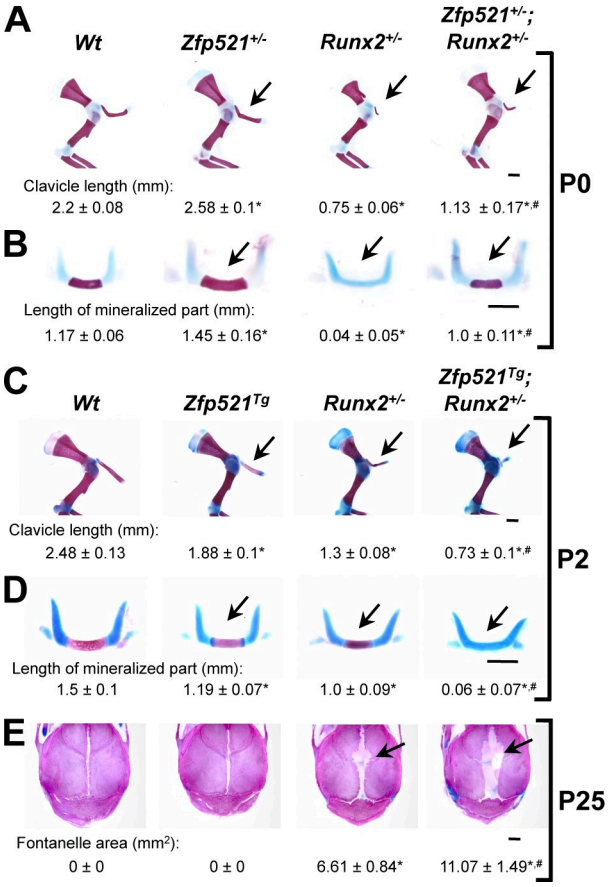

Figure 1. **Zfp521 is a physiological antagonist of Runx2 in vivo.** (A) At postnatal day 0 (P0), *Zfp521*$^{+/-}$ mice present a modestly elongated clavicle compared with *Wt* mice. Runx2$^{+/-}$ mice exhibit a very severe hypoplasia of the clavicle, which is mitigated in *Runx2*$^{+/-}$;*Zfp521*$^{+/-}$ mice (arrows). (B) Compared with *Wt* mice, *Zfp521*$^{+/-}$ mice demonstrate a more strongly mineralized midportion of the hyoid bone. The delayed mineralization of the midportion of the hyoid bone in *Runx2*$^{+/-}$ mice is rescued in *Runx2*$^{+/-}$;*Zfp521*$^{+/-}$ mice (arrows). (C) A progressively severe hypoplasia of the clavicle was seen in postnatal day 2 (P2) *Zfp521*^{Tg} mice, *Runx2*$^{+/-}$ mice, and Zfp521^{Tg};Runx2$^{+/-}$ mice (arrows). (D) The midportion of the hyoid bones of P2 *Zfp521*^{Tg} mice, *Runx2*$^{+/-}$ mice, and *Zfp521*^{Tg};*Runx2*$^{+/-}$ mice show a progressive decrease in size and mineralization (arrows). (E) The calvaria of postnatal day 25 (P25) *Zfp521*^{Tg} mice were similar to the calvaria of *Wt* mice. *Runx2*$^{+/-}$ mice exhibited open anterior and posterior fontanelles and wide cranial sutures, which were strikingly enhanced in *Zfp521*^{Tg};*Runx2*$^{+/-}$ mice (arrows). Skeletal structures were measured. Data are mean ± SEM. *, $P < 0.05$ versus *Wt*. #, $P < 0.05$ versus *Runx2*$^{+/-}$. Littermates were analyzed as controls. Results are representative of six to eight animals. Bars, 1 mm.

Zfp521 antagonizes Runx2 transcriptional activity and early stage osteoblast differentiation, leading to an accumulation of mesenchymal precursor cells

Based on our in vivo observations, we proceeded to analyze the effects of Zfp521 on Runx2 at the cellular and molecular levels. At the cellular level, we determined the expression of Runx2 and its direct target gene *Osx* (Nakashima et al., 2002) in early stage osteoblasts derived from neonatal *Zfp521*$^{+/-}$ and *Zfp521*^{Tg} mice. Consistent with the in vivo findings, *Zfp521*$^{+/-}$ osteoblasts demonstrated a higher expression of Runx2 and Osx compared with control (Fig. 2 A), whereas the expression of both Runx2 and Osx was significantly reduced in osteoblasts constitutively overexpressing Zfp521 (Fig. 2 B). To confirm the repression of Runx2 expression by Zfp521, we analyzed the level of Runx2 protein in osteoblasts from the *Zfp521*^{Tg} mice. Indeed, both immunofluorescence microscopy and immunoblot analysis showed that Runx2 protein was reduced in the osteoblasts derived from *Zfp521*^{Tg} mice (Fig. 2 C).

To further examine the effect of Zfp521 on Runx2 transcriptional activity, we used a luciferase reporter gene driven by six concatenated osteoblast-specific element 2 (OSE2) cassettes (6×OSE2-luc; Ducy and Karsenty, 1995). Zfp521 alone had no effect on the reporter activity but completely blocked the Runx2-mediated promoter activation in a dose-dependent manner, and Runx2 dose-dependently reversed the Zfp521-induced inhibition (Fig. S1 B).

Consistent with the delayed mineralization in vivo, primary calvarial osteoblasts from *Zfp521*^{Tg} mice displayed reduced alkaline phosphatase (ALP) activity (Fig. 2 D). Similarly, Zfp521 repressed ALP activity in osteoblasts (Fig. S1 C) and in MC3T3-E1 cells stably overexpressing Zfp521 (not depicted). This repression was dose-dependently rescued by coinfection with Runx2 adenovirus (Fig. S1 C). Collectively, these results indicate that Zfp521 attenuates Runx2 activity and restricts early osteoblast differentiation.

Runx2 also antagonizes the proliferation of osteoblast precursors (Galindo et al., 2005), which may contribute to the osteoblast phenotype. To determine whether Zfp521 modulates the proliferation of osteoblast precursor cells, we quantified [^{3}H]thymidine incorporation by calvarial cells obtained from *Zfp521*^{Tg} mice and control littermates. Zfp521 had no detectable effect on the thymidine incorporation (Fig. 2 E), suggesting that the reduced osteoblast phenotype seen in our assays was primarily caused by an impaired commitment to the osteoblast lineage and/or to a reduced osteoblast differentiation and not a proliferation-related effect of Zfp521.

Next, we hypothesized that the block in the differentiation of early stage osteoblasts derived from *Zfp521*^{Tg} mice might lead to an increase in the abundance of mesenchymal precursor cells, which would then accumulate. To test this hypothesis, we analyzed the precursor capability of bone marrow stromal cells derived from adult *Zfp521*^{Tg} mice and control littermates using standardized fibroblastic (colony-forming unit–fibroblast [CFU-F]) and mineralizing (colony-forming unit–osteoblast [CFU-OB]) colony-forming unit assays and found that both CFU-F and CFU-OB were indeed increased in Zfp521-overexpressing mice (Fig. 2 F). In summary, these data demonstrate that Zfp521 reduces Runx2 activity and expression and restricts early stage osteoblast differentiation but not proliferation, resulting in an accumulation of mesenchymal precursor cells.

Zfp521 zinc finger (ZF) domains 6 and 26 mediate the interaction with Runx2 and the inhibition of Runx2 transcriptional activity

At the molecular level, coimmunoprecipitation assays showed that Zfp521 associates with Runx2 in osteoblasts not only in an overexpression system (Fig. S2 A; Wu et al., 2009) but also, and more importantly, under endogenous conditions (Fig. 3 A). To identify the Runx2 domains that are required for the interaction

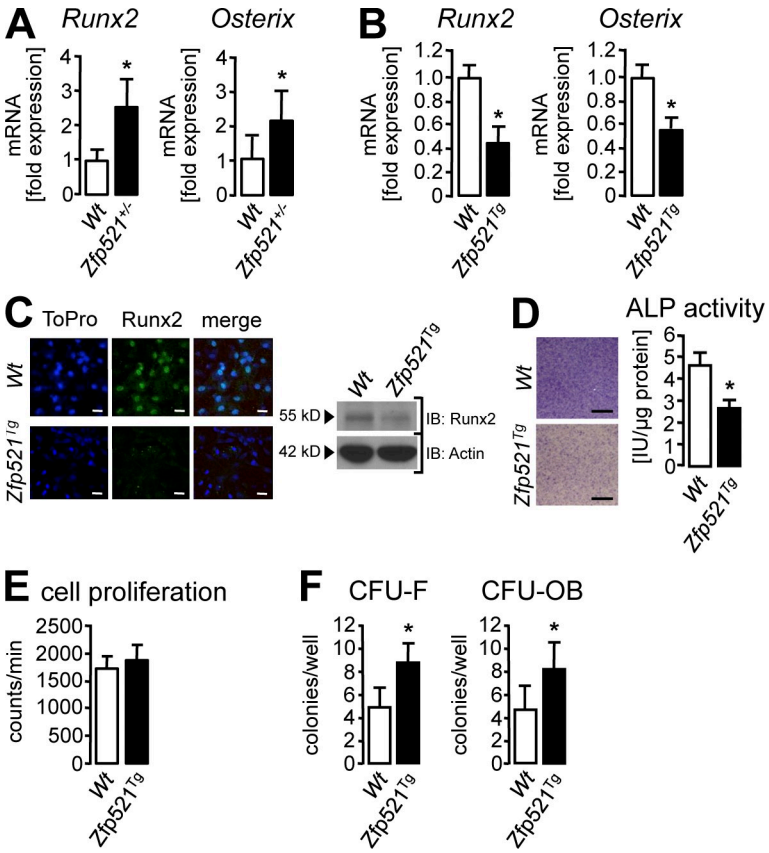

Figure 2. **Zfp521 inhibits early stage osteoblast differentiation and increases the number of osteoprogenitors.** (A) Gene expression analysis revealed that Runx2 and Osx mRNA expression was significantly increased in *Zfp521*$^{+/-}$ neonatal calvarial osteoblasts compared with *Wt* mice. (B) Runx2 and Osx mRNA expression was significantly decreased in calvarial osteoblasts isolated from *Zfp521*^{Tg} mice. (C) Immunostaining and immunoblot (IB) analysis showed reduced Runx2 expression in calvarial osteoblasts from *Zfp521*^{Tg} mice and *Wt* littermates. Nuclei were stained with ToPro. Results are representative of three independent experiments. Bars, 10 µm. (D) Cultured calvarial cells from *Zfp521*^{Tg} mice and control littermates were stained for ALP activity, or the cells were lysed, and ALP activity was determined colorimetrically. ALP activity was reduced in cells overexpressing Zfp521. Bars, 5 mm. (E) [^{3}H]Thymidine incorporation by calvarial osteoblasts from *Zfp521*^{Tg} mice and control littermates showed no changes in osteoblast proliferation. (F) *Zfp521*^{Tg} mice contained an increased number of colony-forming unit–fibroblast (CFU-F) and colony-forming unit–osteoblast (CFU-OB). All results are representative of three to eight animals. All data are shown as mean ± SEM. *, $P < 0.05$ versus *Wt*.

with Zfp521, we expressed a series of progressively truncated Runx2 fragments that together encompass the entire Runx2 molecule in HEK-293 cells and determined which fragments bound to a GST-Zfp521 fusion protein (Fig. 3 B). Immunoblot analysis revealed that Zfp521 interacted with Runx2 fragments that contained the Runt and the QA domain but not with the isolated repressor domain.

We then investigated the features of Zfp521 that mediate the Runx2–Zfp521 interaction. Because ZF-mediated interactions often depend on the zinc ion–stabilized conformation of the ZF domain (Turner and Crossley, 1999), we first tested how chelating the zinc ions affected the Zfp521–Runx2 interaction. Removing the zinc ions significantly reduced the interaction of Zfp521 with Runx2 (Fig. 3 C).

To identify the ZF domains that interact with Runx2, we analyzed the binding of Runx2 to a series of fragments that spanned the entire length of Zfp521 (Fig. 3 D). Runx2 bound strongly to the fragments that comprised ZFs 6–10 and ZFs 26–30 and, to a lesser degree, with the ZF 21–25 fragment, suggesting that Zfp521 contains at least two Runx2-interacting sites, one located near the N terminus and the other near the C terminus.

We next generated a library of constructs in which the ZF histidines of the ZF 6–10 and ZF 26–30 fragments were randomly mutated to glutamic acid, abolishing the zinc ion coordination and destabilizing the conformation of the mutated ZFs. We found the ZF 6–10 fragments with an intact ZF 6 coimmunoprecipitated with Runx2, regardless of whether ZFs 7–10 were mutated, whereas those with a mutation in ZF 6 did not interact (Fig. 3 E). Similarly, only the ZF 26–30 fragments with an intact ZF 26 associated with Runx2 (Fig. 3 F).

To determine whether destabilizing the conformations of ZFs 6 and 26 was sufficient to disable the binding of the full-length Zfp521 to Runx2, the zinc-coordinating histidine residues of ZF domains 6 and 26 (H^{264}, H^{269}, H^{1156}, and H^{1161}) were mutated to glutamic acid. Coimmunoprecipitation of Wt Runx2 and full-length Zfp521 bearing disabled ZF domains 6 and 26 revealed a greatly reduced association of the two molecules (Fig. S2 B).

We then examined how disabling the zinc coordination of the ZF 6 and ZF 26 domains affected Zfp521's ability to antagonize Runx2-dependent transactivation of the 6×OSE2-luc reporter assay. As before, Wt Zfp521 completely abolished the Runx2-mediated promoter activation. In contrast to the complete inhibition by the Wt protein, the mutated Zfp521 reduced the Runx2-induced reporter activity by ∼50% (Fig. 3 G), indicating the functional importance of these two domains. Similar results were obtained using the Osteocalcin promoter-driven luciferase (OG2-luc) reporter (unpublished data).

Zfp521 antagonizes Runx2 activity in an HDAC3-dependent manner

In identifying the mechanism by which Zfp521 antagonizes Runx2 activity, we first examined its effect on the binding of Runx2 to DNA. Coexpressing Zfp521 had no effect on the ability of Runx2 to bind to oligonucleotides that contained either the rat Osteocalcin promoter OG2 response element or the mouse Osteocalcin promoter OSE2 response element (Fig. 4 A; Ducy and Karsenty, 1995), indicating that Zfp521 does not

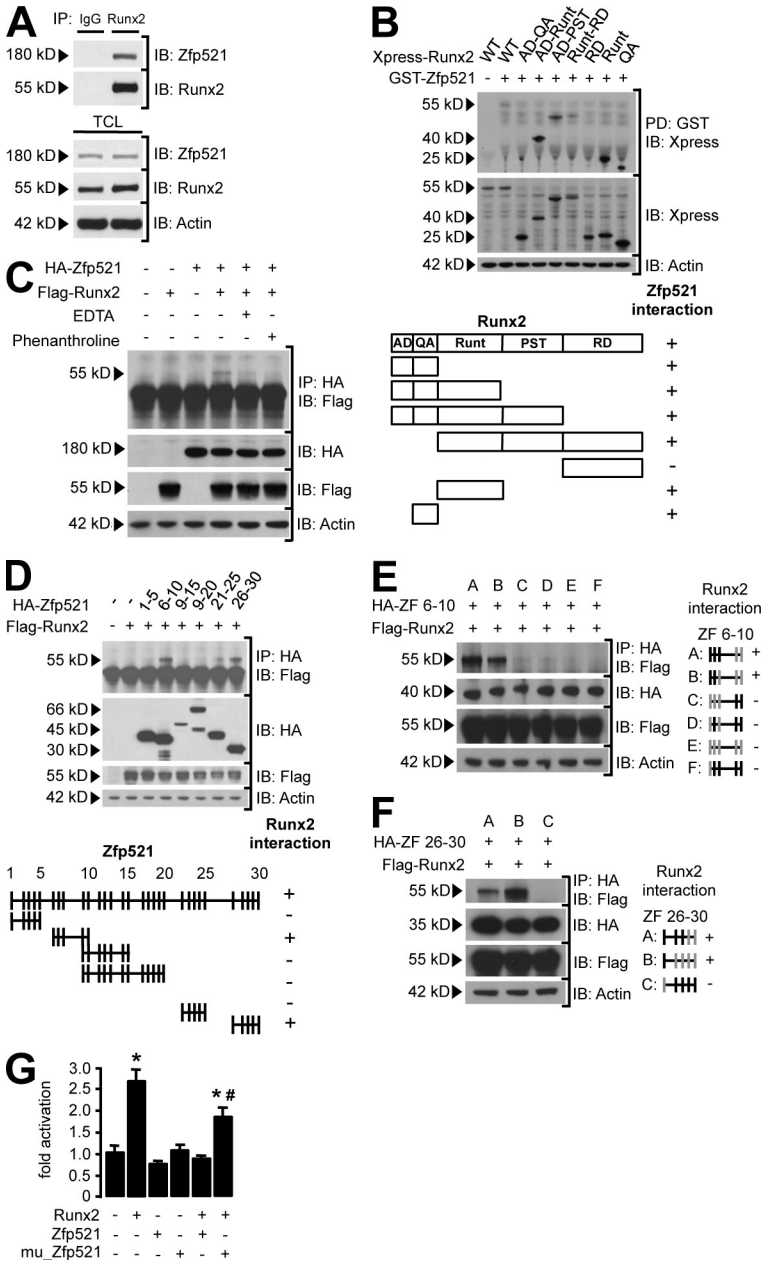

Figure 3. **Structure–function analysis of the Zfp521–Runx2 interaction.** (A) Runx2 was immunoprecipitated (IP) from lysate of *Wt* calvarial osteoblasts, and the immune complexes were immunoblotted (IB) for Zfp521 and Runx2. Nonimmune IgG was the immunoprecipitated control. Presence of Zfp521 and Runx2 in total cell lysate (TCL) is shown. (B) Wild-type (WT) Xpress-Runx2 and fragments of Runx2 were overexpressed in HEK-293 cells, and the binding to immobilized GST-Zfp521 was determined by pull-down (PD) followed by immunoblotting (top). The expression of Runx2 proteins was confirmed by immunoblotting of cell lysates (middle). The schematic drawing shows Runx2 domains (AD, QA, Runt, PST, and RD) and the truncated forms. The binding of each fragment is indicated. (C) Chelating zinc ions with either EDTA or phenanthroline abolished the interaction of Flag-Runx2 with HA-Zfp521. HA-Zfp521 was immunoprecipitated with anti-HA in HEK-293 cells, and the immune complex was immunoblotted for Flag-Runx2 using anti-Flag antibody. (D) HA-tagged fragments of Zfp521 containing five zinc fingers (ZFs) each were constructed as shown in the schematic drawing. Each fragment was overexpressed (second panel, cell lysate) along with Flag-Runx2 (third panel, cell lysate) in HEK-293 cells and subjected to coimmunoprecipitation (top). Runx2 bound to the fragments containing ZFs 6–10 and 26–30 (summarized next to schematic drawing). (E and F) Zinc-coordinating His residues in fragments ZF 6–10 (E) and ZF 26–30 (F) were randomly mutated to disrupt individual ZF conformation. HA-tagged Zfp521 fragments with complementary disabled ZFs (marked in gray in the schematic drawings) and Flag-Runx2 were overexpressed in HEK-293 cells. Cell lysates were blotted for HA (second panels) or Flag (third panels). Binding of the mutated fragments to Runx2 is indicated. (G) ZFs 6 and 26 were disabled in full-length Zfp521 (mu_Zfp521). Neither Wt Zfp521 nor mu_Zfp521 alone affected the 6×OSE2-luc activity. In contrast to Wt Zfp521, mu_Zfp521 only partially antagonized Runx2 activity. Actin was used as a loading control in A–F. All results are representative of three to five independent experiments. Data are mean ± SEM. *, $P < 0.05$ versus control. #, $P < 0.05$ versus Runx2.

repress Runx2 activity by preventing the association of Runx2 with its consensus DNA binding site, the mechanism used by Twist, another Runx2 antagonist that regulates skeletogenesis (Bialek et al., 2004).

We then considered the possibility that Zfp521 could recruit the repressor machinery to Runx2. HDACs antagonize Runx2 activity (Westendorf et al., 2002; Schroeder et al., 2004; Kang et al., 2005; Jensen et al., 2008, 2009), and a conserved motif encoding the first 13 amino acids at the N terminus of early hematopoietic ZF protein, the human homologue of Zfp521, binds the nucleosome remodeling and HDAC (NuRD) complex, which contains HDAC1, HDAC2, MTA2, and RbAp48 (Bond et al., 2008). We therefore hypothesized that Zfp521 antagonizes Runx2 activity by recruiting HDACs to the transcription complex. Consistent with this hypothesis, the class I and class II HDAC inhibitor trichostatin A (TSA) completely blocked the repression of Runx2-induced 6×OSE2-luc reporter activity by Zfp521 but had little effect on Runx2 alone (Fig. 4 B), implicating HDACs in the Zfp521-induced repression of Runx2.

To determine whether Zfp521 repressed Runx2 activity by recruiting the HDAC-containing NuRD complex, we deleted the NuRD binding site and confirmed that the truncated protein (Δ13Zfp521) failed to interact with components of the NuRD complex (Fig. S3 A). The truncated mutant repressed the Runx2-induced 6×OSE2-luc reporter gene activity to the same extent as Wt Zfp521 (Fig. 4 C), indicating that the NuRD complex does not participate in the Zfp521-mediated repression of Runx2.

Because HDAC5, which is not part of the NuRD complex, also antagonizes Runx2 (Kang et al., 2005), we next tested the function of Zfp521 in rat osteosarcoma cell line (ROS) cells that stably express a dominant-negative form of HDAC5

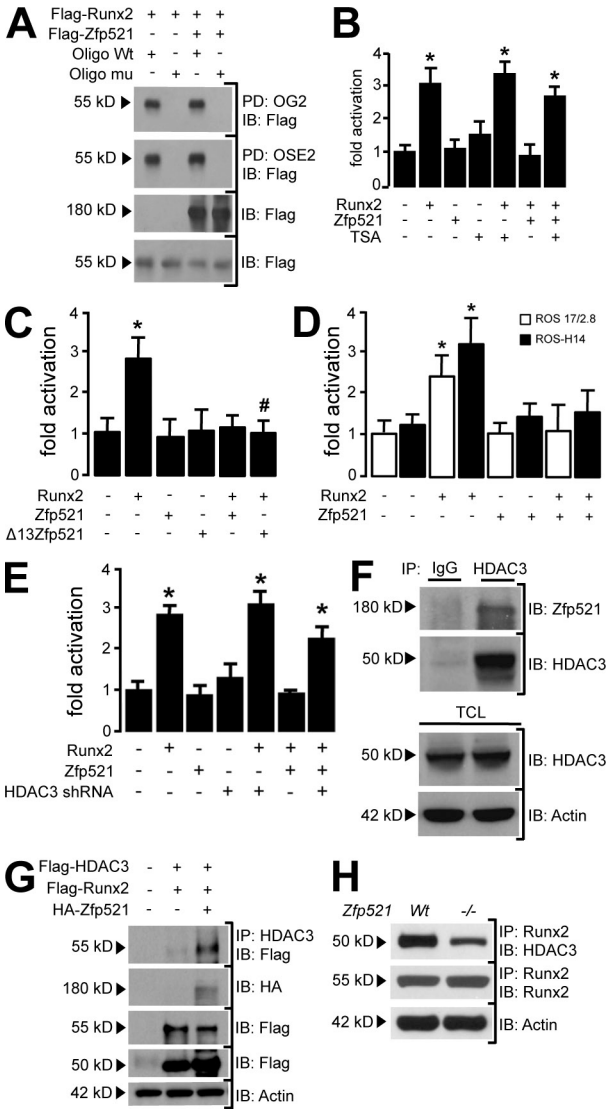

Figure 4. **Zfp521 represses Runx2 activity in an HDAC3-dependent manner.** (A) Pull-down (PD) of Flag-Runx2 was performed in the absence or presence of Flag-Zfp521 using biotinylated oligonucleotides (Oligo; wild type [Wt] or mutated [mu]) encoding Runx2 consensus sites (rat [OG2] or mouse [OSE2] Osteocalcin promoter). Oligonucleotide-bound Flag-Runx2 was immunoblotted (IB) using anti-Flag antibody. HEK-293 cell lysates were analyzed by immunoblotting for overexpressed Flag-Runx2 and Flag-Zfp521. (B) Zfp521 prevented Runx2 from activating the 6×OSE2-luc reporter in ROS cells. The HDAC inhibitor trichostatin A (TSA) had little effect on the reporter alone or Runx2-induced activity but abolished Zfp521's repression of Runx2-induced activity. (C) Δ13Zfp521 repressed the Runx2-driven 6×OSE2-luc reporter activity in ROS cells as well as full-length Zfp521. (D) Zfp521 fully reversed the Runx2-mediated 6×OSE2-luc reporter gene activation in Wt ROS cells (ROS17/2.8) and in ROS cells overexpressing a dominant-negative form of HDAC5 (ROS-H14). (E) Depleting endogenous HDAC3 using shRNA abolished the repression of Runx2-induced 6×OSE2-luc reporter gene activity by Zfp521. (F) Anti-HDAC3 coimmunoprecipitates (IPs) Zfp521 and HDAC3 from *Wt* calvarial osteoblast lysate. Nonimmune IgG was used as a control. HDAC3 is present in total cell lysate (TCL) as determined by immunoblotting. (G) Flag-HDAC3 was immunoprecipitated with anti-HDAC3 in ROS cells, and the immune complex was immunoblotted for Flag-Runx2 with anti-Flag antibody. (H) Endogenous Runx2 was immunoprecipitated from calvarial osteoblasts from *Wt* mice, or mice germline was deleted of *Zfp521* (−/−), and endogenous HDAC3 and Runx2 were detected by immunoblotting. The interaction between Runx2 and HDAC3 was greatly reduced in osteoblasts lacking *Zfp521*. Actin was used as loading control in F–H. In B–E, results are shown as mean ± SEM. *, $P < 0.05$ versus control. #, $P < 0.05$ versus Runx2. P-values are representative of three to five independent experiments.

(Kang et al., 2005). Zfp521 still retained its full repressive effect on Runx2 activity in these cells (Fig. 4 D), thereby excluding HDAC5 as a component of the mechanism.

HDAC3, another class I HDAC, also interacts with and antagonizes Runx2, leading to an inhibition of early osteoblast differentiation (Schroeder et al., 2004), much like the effect of Zfp521. We therefore explored the role of HDAC3 in Zfp521's repression of Runx2 by depleting HDAC3 in ROS cells using a short hairpin RNA (shRNA; Fig. S3 B) and found that depleting HDAC3 largely prevented the repression of Runx2-induced reporter activity by Zfp521 (Fig. 4 E), indicating that HDAC3 indeed plays a role in the repression of Runx2 activity by Zfp521. Consistent with Zfp521 recruiting HDAC3 to a transcriptional repressor complex with Runx2, Zfp521 coimmunoprecipitated with both endogenous and overexpressed HDAC3 (Fig. 4 F and Fig. S3 C). Most importantly, overexpressing Zfp521 in osteoblasts enhanced the association of HDAC3 and Runx2 (Fig. 4 G), whereas genetic ablation of *Zfp521* reduced it to a great extent (Fig. 4 H). Thus, Zfp521 appears to act as a functionally important adaptor protein, interacting with both Runx2 and HDAC3 and enhancing the association of the two proteins, thereby repressing Runx2 transcriptional activity.

Reversal of the skeletal abnormalities in Runx2-overexpressing mice by Zfp521

Although Runx2 is indispensable for the commitment of mesenchymal precursor cells to the osteoblast lineage (Ducy et al., 1997; Komori et al., 1997), a sustained high level of Runx2 appears to exert a maturational block on differentiating osteoblasts, leading to reduced bone formation and an osteoblast-dependent increase in osteoclastogenesis and bone resorption, culminating in a low bone mass with long-bone fractures in adult mice (Liu et al., 2001; Geoffroy et al., 2002). We therefore used the Runx2-antagonistic properties of Zfp521 to determine whether repression of Runx2 would reverse the osteopenia in this model.

The *Zfp521*^{Tg} mice were crossed with mice overexpressing Runx2 under the control of the 2.3-kb fragment of the rat Collagen I type 1 (Col1) promoter (*Runx2*^{Tg} mice; Geoffroy et al., 2002) to establish double-transgenic *Zfp521*^{Tg};*Runx2*^{Tg} mice. The rat Col1-2.3kb promoter is active in cells of the osteoblast lineage, foremost at the committed matrix-producing differentiation stage (Geoffroy et al., 2002). The concurrent activity of the ENO2 promoter driving the overexpression of Zfp521 and the Col1-2.3kb promoter controlling the ectopic expression of Runx2 was confirmed in the long bones of adult mice (Fig. S4, A and B).

Histomorphometric analysis revealed that *Zfp521*^{Tg} mice had a high bone mass phenotype with a significant increase in bone volume per tissue volume (BV/TV) and bone formation seen in tibiae (Fig. 5 A) and lumbar vertebrae (Fig. S5). In contrast, and as previously reported (Geoffroy et al., 2002), histomorphometric analysis of proximal tibiae of *Runx2*^{Tg} mice revealed a strikingly low bone mass phenotype characterized by a low BV/TV, a reduced bone formation rate, and increased numbers of osteoblasts and osteoclasts in the trabecular bone region (Fig. 5 A). The cortical bone in tibiae of *Runx2*^{Tg} mice was thin, which was at least in part caused by a reduced cortical mineral

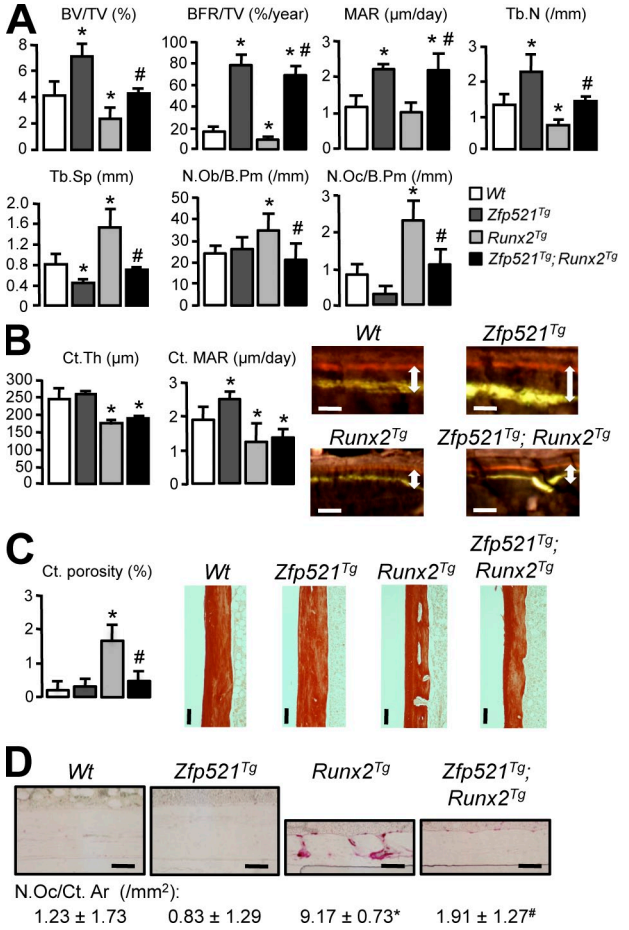

Figure 5. **Zfp521 reverses the low bone mass in *Runx2*^{Tg} mice.** Phenotypic characterization of 5-wk-old *Wt*, *Zfp521*^{Tg}, *Runx2*^{Tg}, and *Zfp521*^{Tg};*Runx2*^{Tg} female mice is shown. (A) Histomorphometric analysis of the trabecular bone in proximal tibiae (bone volume/tissue volume [BV/TV], bone formation rate/tissue volume [BFR/TV], mineral apposition rate [MAR], trabecular number [Tb.N], trabecular separation [Tb.Sp], number of osteoblasts/bone perimeter [N.Ob/B.Pm], and number of osteoclasts/bone perimeter [N.Oc/B.Pm]) demonstrates the normalization of the low bone mass of *Runx2*^{Tg} mice by Zfp521. (B) Analysis of the cortical thickness (Ct.Th) in the tibia midshaft. Cortical mineral apposition rate (Ct.MAR) was determined by calcein/democycline double labeling (double arrows). Bars, 20 µm. (C) Cortical porosity (Ct. porosity) was quantified using Sirius red–stained decalcified paraffin-embedded cortical sections. Bars, 100 µm. (D) Tartrate-resistant acid phosphatase staining of decalcified paraffin-embedded cortical sections shows increased numbers of osteoclasts and resorption in the cortical bone of *Runx2*^{Tg} mice compared with *Zfp521*^{Tg} and *Wt* mice, which was normalized by Zfp521. Ct.Ar., cortical area. Bars, 100 µm. Data are mean ± SEM. n = 4–6 mice per group. *, $P < 0.05$ versus *Wt*. #, $P < 0.05$ versus *Runx2*^{Tg}.

apposition rate (Fig. 5 B). In addition, the cortices were highly porous (Fig. 5 C), consistent with an increased number of active osteoclasts in the cortex (Fig. 5 D). Analysis of *Zfp521*^{Tg};*Runx2*^{Tg} double-transgenic mice revealed that overexpression of Zfp521 reversed all aspects of the phenotype of the *Runx2*^{Tg} mice (Fig. 5, A, C, and D) except for the cortical mineral apposition rate and cortical thickness, which remained low (Fig. 5 B).

A key feature of the bone phenotype of *Runx2*^{Tg} mice is that osteoblast maturation is blocked (Liu et al., 2001; Geoffroy et al., 2002). Consistent with this, we observed an accumulation of rather immature Osteopontin-positive osteoblasts (Fig. 6 A) and a reduced number of Osteocalcin-expressing mature osteoblasts (Fig. 6 B) and Dentin matrix protein 1 (Dmp-1)–positive osteocytes (Fig. 6 C) in the *Runx2*^{Tg} bones, which was reversed by overexpressing Zfp521. To confirm the restored osteoblast differentiation, the expression of Dmp-1 was quantified in the cortical bone of the same animals (Fig. 6 D). We therefore concluded that a sustained high level of Runx2 expression indeed leads to a block of osteoblast maturation. Moreover, overexpressing Zfp521 removes this block, allowing osteoblasts to complete differentiation and restoring the number of osteocytes in the cortex.

The increased bone resorption in *Runx2*^{Tg} mice results from an osteoblast-dependent increase in osteoclastogenesis caused by an increase in the ratio of the osteoblast-derived and osteoclast-stimulating receptor activator for nuclear factor κB ligand (Rankl) and the osteoblast-derived soluble Rankl decoy receptor Osteoprotegerin (Opg; Geoffroy et al., 2002). We confirmed that the Rankl/Opg ratio was doubled in bones derived from *Runx2*^{Tg} mice and this increase was normalized in the *Zfp521*^{Tg};*Runx2*^{Tg} mice (Fig. 6 E), consistent with the normalized number of less mature osteoblasts (Fig. 5 A and Fig. 6 A), which are the main sources of Rankl (Giner et al., 2008).

As a consequence of their strikingly reduced bone mass, *Runx2*^{Tg} mice ultimately developed fractures in the midshaft region of the tibia (Fig. 6 F) and, less frequently, of the femur and the tail vertebrae (not depicted). The ambulatory activity of the mice was not compromised, and fracture healing occurred, as demonstrated by a callus formation (Fig. 6 F). To compare the severity of the fracture phenotype, we established a fracture rate (the mean number of hind-limb fractures per animal) for mice of each genotype. *Zfp521*^{Tg};*Runx2*^{Tg} mice showed an 80% reduced fracture rate compared with *Runx2*^{Tg} mice (Fig. 6 F), presumably owing to the restoration of both bone mass and cortical porosity. In summary, Zfp521 overexpression normalized most of the phenotypic alterations observed in *Runx2*^{Tg} mice, demonstrating that Zfp521 can also antagonize Runx2 activity at later stages of osteoblast differentiation.

Discussion

Commitment of mesenchymal precursor cells to the osteoblast lineage and subsequent osteogenic development involve a tightly regulated differentiation program. After commitment, cells pass through early differentiation stages to become bone-forming osteoblasts and finally reach a terminally differentiated stage (Hartmann, 2009) in which they exit the cell cycle and either undergo apoptosis, become a bone-lining cell, or adopt the fate of a matrix-entrapped osteocyte (Harada and Rodan, 2003). Normal bone homeostasis requires balancing the ongoing commitment of sufficient numbers of preosteoblasts with the maintenance of self-renewing precursors for future osteogenic differentiation (Moore and Lemischka, 2006; Kolf et al., 2007) as well as appropriately regulating the rates of early and late differentiation. Any imbalance of this system can positively or negatively affect the skeletal phenotype.

At the molecular level, many transcription factors and a variety of coregulators control the progression of mesenchymal precursor cells toward terminally differentiated osteoblasts with

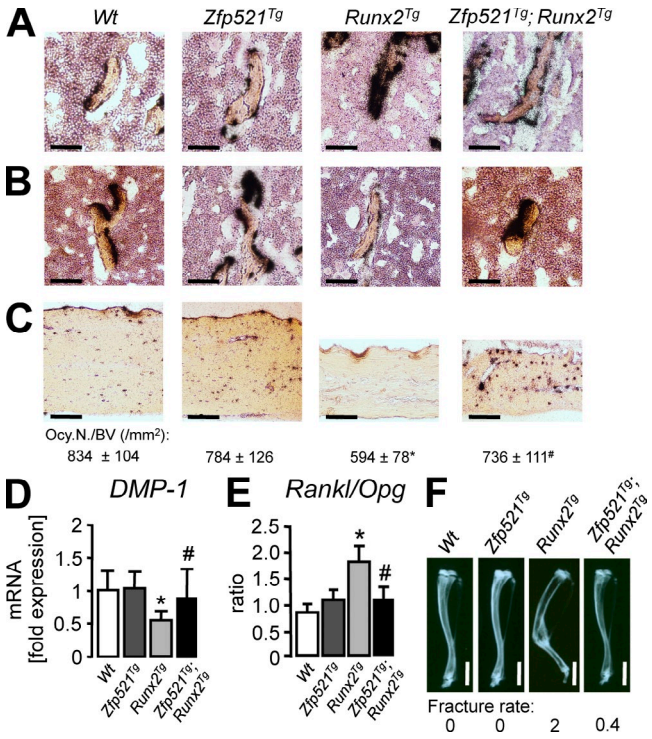

Figure 6. **Zfp521 relieves the Runx2-induced block of osteoblast maturation.** (A–C) Expression of osteopontin (A), osteocalcin (B), and dentin matrix protein 1 (Dmp-1; C) was determined by in situ hybridization of decalcified tibiae. In the trabecular bone of *Runx2*^{Tg} mice, partially differentiated Osteopontin-expressing osteoblasts were increased, and mature Osteocalcin-expressing osteoblasts were decreased compared with *Zfp521*^{Tg} and *Wt* littermates, as were Dmp-1–expressing osteocytes in the cortical bone. Overexpressing Zfp521 normalized the number of Osteopontin-positive cells and restored the abundance of mature osteoblasts and osteocytes in *Zfp521*^{Tg}*;Runx2*^{Tg} mice. The number of osteocytes in the cortical bone was determined per bone volume (Ocy.N./BV). Bars, 100 µm. (D) Changes in the number of osteocytes were confirmed by quantifying Dmp-1 mRNA expression in the cortical bones of the same animals. (E) The increased Rankl/Opg ratio in 5-wk-old female *Runx2*^{Tg} mice was normalized in *Zfp521*^{Tg}*;Runx2*^{Tg} animals. (F) Radiograms of the right tibia of 12-wk-old male mice. *Runx2*^{Tg} mice had a mean of two midshaft fractures in hind-limb long bones (fracture rate). The fracture rate was reduced by 80% in *Zfp521*^{Tg}*;Runx2*^{Tg} animals. Bars, 2.5 mm. All data are mean ± SEM. n = 4–6 mice per group. *, $P < 0.05$ versus *Wt*. #, $P < 0.05$ versus *Runx2*^{Tg}.

Runx2 playing a central role (Lian et al., 2006; Hartmann, 2009). A rise in Runx2 transcriptional activity is a prerequisite for the transition of a mesenchymal precursor cell to an osteoprogenitor cell (Ducy et al., 1997). In humans, some *Runx2* mutations cause CCD (Mundlos et al., 1997), a syndrome that is largely recapitulated in *Runx2*$^{+/-}$ mice (Otto et al., 1997). Because the proper development of intramembranous bone is very sensitive to changes in Runx2 activity (Lou et al., 2009), Runx2 activity must be tightly controlled in both a positive and negative fashion. On the other hand, overexpressing Runx2 in more mature osteoblasts inhibits osteoblast maturation and matrix protein production (Liu et al., 2001; Geoffroy et al., 2002), indicating that Runx2 plays different roles depending on the stage of osteoblast differentiation.

Zfp521 is a recently identified transcriptional coregulator that antagonizes Runx2 transcriptional activity in vitro (Wu et al., 2009). This interesting and potentially biologically relevant finding, together with the complex role of Runx2 during osteoblast differentiation, led us to analyze the functional consequences of altering the relative levels of Runx2 and Zfp521 on early and late stages of bone development and homeostasis, specifically examining the effects of altering Zfp521 levels during early development on the CCD phenotype of *Runx2*$^{+/-}$ mice and at later stages on the osteopenic phenotype of the *Runx2*^{Tg} mouse.

Our results provide genetic evidence that Zfp521 antagonizes the early developmental osteogenic function of Runx2 in vivo. Eliminating one *Zfp521* allele in *Runx2*$^{+/-}$ mice partially rescued the CCD phenotype, whereas overexpressing Zfp521 in the *Runx2*$^{+/-}$ mice exacerbated the CCD phenotype, delaying osteoblast differentiation and subsequent matrix mineralization. We also found that overexpressing Zfp521 antagonized most, but not all, of the negative effects of Runx2 during later bone growth and homeostasis. The diminished trabecular bone formation and bone mass, as well as the increased osteoclastogenesis and porosity seen in the cortex of *Runx2*^{Tg} mice, were fully reversed in *Zfp521*^{Tg}*;Runx2*^{Tg} mice, and the fracture rate was greatly reduced. However, Zfp521 failed to restore the thin cortical bone found in *Runx2*^{Tg} mice, perhaps owing to a mineral apposition rate that was less increased in cortical than in trabecular bone. Thus, cortical and trabecular bone appear to be differently regulated, as has been shown in other instances (Compston, 2007). Collectively, these data demonstrate that Zfp521 antagonizes both Runx2-induced osteogenic commitment of mesenchymal precursors and the Runx2-induced block of osteoblast maturation.

In vitro, Zfp521 dose-dependently antagonized Runx2 transcriptional activity and Runx2-mediated early stage osteoblast differentiation. Although Runx2 is implicated in cell cycle regulation (Galindo et al., 2005), Zfp521 did not appear to modulate proliferation in osteoblasts. Thus, by limiting the progression of osteoblast differentiation, Zfp521 maintains the pool of mesenchymal precursors and early committed osteoblasts, as shown by the increased numbers of colony-forming units in the marrow of the Zfp521-overexpressing mice. Together, these findings suggest that the antagonism of Runx2 by Zfp521 reduces the commitment and/or early differentiation of osteoprogenitors cells while promoting osteoblast maturation and increasing bone mass in vivo. They do not, however, exclude the possibility that Zfp521 may also increase bone mass by affecting other factors that regulate bone homeostasis. For instance, Zfp521 has been reported to repress early B cell factor 1 (Ebf1) activity in vitro (Bond et al., 2004), and deletion of *Ebf1* leads to an increase in bone formation (Hesslein et al., 2009).

In vitro analysis revealed that Zfp521 binds to Runx2 within the QA and Runt domains and identified two Zfp521 ZF domains (6 and 26) that are critical for this interaction. Mutating the Zn^{2+}-coordinating His residues of these ZFs and thereby destabilizing the ZF conformation reduced both the binding of Zfp521 to Runx2 and the Zfp521-mediated repression of Runx2 transcriptional activity, confirming the functional importance of the association of Zfp521 and Runx2. The residual binding could result from partial stabilization of the ZF domain conformations in the context of full-length Zfp521, from the presence of other Runx2 binding sites that were not apparent in the

fragments, and/or from the stabilization of the Zfp521–Runx2 interaction by other factors that function as adaptor molecules in a larger complex.

Several HDACs have been reported to reduce Runx2 transcriptional activity (Westendorf et al., 2002; Schroeder et al., 2004; Kang et al., 2005; Jensen et al., 2008, 2009). Although Zfp521 attenuates Runx2 activity via HDAC4 in chondrocytes (Correa et al., 2010), this study indicates that, in osteoblasts, Zfp521 antagonizes Runx2 activity at least in part by recruiting HDAC3 to the Runx2 transcriptional complex. Inhibition of class I and class II HDACs prevented the Zfp521-induced blockade of Runx2 transcriptional activity, as did the depletion of HDAC3 specifically. In contrast to the requirement for HDAC3, Zfp521's negative effect on Runx2 appears to be independent of HDAC5, which also represses Runx2 (Kang et al., 2005) and the HDAC1- and HDAC2-containing NuRD complex, which binds to a motif at the N terminus of Zfp521 (Bond et al., 2008). The interaction between Runx2 and HDAC3 was strikingly enhanced by Zfp521. In addition, genetic ablation of *Zfp521* strongly reduced the association of Runx2 and HDAC3. Our conclusion that Zfp521 promotes the association of HDAC3 and Runx2 is further supported by the location of the Zfp521 binding site within the QA and Runt domains of Runx2 because these domains have been reported to harbor a TSA-sensitive autonomous repression domain and function as a binding site for HDAC3 (Schroeder et al., 2004). The concept of HDAC3 playing a positive role in bone mass accrual despite its negative effect on Runx2 activity is further demonstrated by a recent study describing the osteoblast-targeted deletion of *HDAC3*, causing an impaired intramembranous and endochondral bone formation (Razidlo et al., 2010).

Interestingly, Runx2 is not the only regulatory protein to exert apparently opposite stage-specific effects during osteoblast differentiation. Like Runx2, the transcription factor Snail1 is necessary for the early steps of osteoblast development, but its sustained activity in transgenic mice impairs osteoblast differentiation (de Frutos et al., 2009). Similarly, high canonical Wnt-signaling activity impairs late-stage osteoblast differentiation and/or function (Li et al., 2005; van der Horst et al., 2005; Rodda and McMahon, 2006), notwithstanding the fact that the canonical Wnt pathway facilitates the commitment of mesenchymal precursor cells to the osteoblast lineage and supports the function of early stage osteoblasts. In addition, TGF-β signaling is important in the maintenance and expansion of the mesenchymal progenitor cells but inhibits differentiation along the osteoblast lineage (Derynck and Akhurst, 2007). Together with these studies, our data reinforce the emerging concept that factors that favor the entry and progression of precursors to the osteoblast lineage might need to be repressed at later stages of differentiation to allow the final steps of osteoblast differentiation and matrix production. Zfp521 appears to play an important role in these later events.

In conclusion, we propose a model in which Zfp521 antagonizes Runx2 activity at both early and late stages of osteoblast differentiation (Fig. 7), thereby both maintaining the number of mesenchymal precursor cells and promoting final osteoblast maturation, respectively. The repression that Zfp521 exerts on Runx2 may therefore contribute to the physiological regulation of skeletal development and adult bone mass in mice.

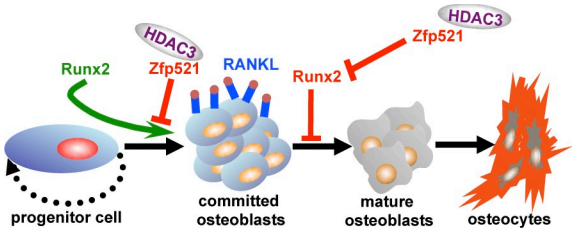

Figure 7. **Model of the regulation of osteoblast differentiation by Zfp521.** Zfp521 interacts with HDAC3 and Runx2, stabilizing the association of these two factors. This corepressor complex represses target gene transcription. Runx2 is required for entry of progenitor cells to the osteoblast lineage. Zfp521 antagonizes this early positive effect of Runx2, leading to decreased osteoblast differentiation and an increased number of progenitors. Committed osteoblasts express Rankl and stimulate osteoclastogenesis. Runx2 antagonizes later stages of osteoblast differentiation, blocking osteoblast maturation. This block leads to an increase of Rankl-expressing immature osteoblasts and therefore to an increase in bone resorption, a decrease in the abundance of terminally differentiated osteoblasts and osteocytes, and ultimately fractures in *Runx2*^{Tg} mice. Zfp521 also antagonizes this later negative effect of Runx2, thereby removing the maturational block and rescuing the low bone mass of *Runx2*^{Tg} mice. The high bone mass phenotype of *Zfp521*^{Tg} mice suggests that Zfp521 exerts a greater effect on Runx2 activity at the later stage of osteoblast differentiation.

Materials and methods

Plasmids

Flag-Runx2 (MASNSL isoform), 6×OSE2-luc (both provided by P. Ducy, Columbia University, New York, NY), Flag-HDAC3, pSHAG-HDAC3 shRNA, scrambled control plasmids (all provided by J. Westendorf, Mayo Clinic, Rochester, MN), and HA-Zfp521 were described previously (Ducy et al., 1997; Schroeder et al., 2004; Wu et al., 2009). A cDNA encoding Zfp521 was generated by PCR and cloned between the Sal1–Not1 sites of the pGEX-4T-1 vector (GE Healthcare) to obtain GST-Zfp521. The vector encoding Flag-Zfp521 or Flag-Δ13Zfp521 was constructed by amplifying Wt Zfp521 or Zfp521 lacking the N-terminal 13 amino acids using pairs of annealing oligonucleotides. The products were subcloned into the Sal1–BamH1 site of the 3×Flag-BICEP-CMV-2 vector (Sigma-Aldrich). HA-Zfp521Δ13 was generated by subcloning the PCR product into the Sal1–BamH1 site of the pCMV5-HA vector (Sigma-Aldrich). HA-tagged constructs encoding several ZF domains (ZF 1–5, ZF 6–10, ZF 9–15, ZF 9–20, ZF 21–25, and ZF 26–30) were amplified by PCR, and the products were cloned between the Sal1–Not1 sites of the pCMV-HA vector (Takara Bio Inc.). Zinc-coordinating His residues of up to five ZFs of the ZF 6–10 and ZF 26–30 fragments were simultaneously randomly mutated to Glu using the multisite-directed mutagenesis kit (QuickChange; Agilent Technologies) according to the manufacturer's instructions, producing constructs with one or both histidines converted to glutamate in one to five of the ZFs. ZF 6 and ZF 26 residues H^{264}, H^{269}, H^{1156}, and H^{1161} were mutated to E in full-length Zfp521 by site-directed mutagenesis. Several fragments of Runx2 encoding individual domains or small groups of domains were amplified from the pCMV-Flag-Runx2 construct by PCR and subcloned in the pcDNA3.1 vector (Invitrogen). All PCR-generated constructs were confirmed by sequencing.

Cell cultures

ROS17/2.8 cells, ROS-H14 (both provided by R. Derynck, University of California, San Francisco, San Francisco, CA), primary calvarial osteoblasts, MC3T3-E1 cells, and HEK-293 cells were cultured in α-MEM with 10% FBS, 100 U/ml penicillin, and 100 µg/ml streptomycin (all obtained from Invitrogen). To induce osteogenic differentiation of primary calvarial osteoblasts, culture medium was supplemented with 50 µM ascorbic acid and 5 mM β-glycerolphosphate (Sigma-Aldrich).

Gene transfections

FuGENE 6 transfection reagent (Roche) was used for transient transfections using a 3:2 FuGENE 6/DNA ratio according to the manufacturer's recommendations.

Virus production and infection experiments

Construction of Runx2 and lacZ adenoviruses was previously described (Wu et al., 2009). To generate adenovirus encoding Zfp521, Zfp521 was

amplified from the pCMV-HA-Zfp521 construct by PCR. The PCR product was cloned between the HindIII–EcoRV sites of the pShuttle-CMV vector (Qbiogene), and virus production was performed as previously described (Wu et al., 2009). MC3T3-E1 cells and primary calvarial osteoblasts from Wt mice were seeded at a density of 5×10^4 cells per well in 6-well tissue culture plates. At 80% confluence, cells were infected with adenoviruses encoding Zfp521 and Runx2 as indicated. Virus encoding lacZ was used to equalize the amount of infectious particles.

Immunoprecipitation

HEK-293 cells were plated at a density of 8×10^5 cells per 10-cm tissue culture dish and grown to 70–80% confluence. 2 µg HA-Zfp521 or 2 µg of any HA-Zfp521–derived mutant, 1 µg Flag-Runx2, and 1 µg Flag-HDAC3 were transfected into HEK-293 cells. After 48 h, cells were lysed in modified radioimmunoprecipitation assay (mRIPA) buffer (50 mM Tris-HCl, pH 7.5, 150 mM NaCl, 1% IGEPAL CA-630 [Sigma-Aldrich], 0.25% deoxycholic acid, 1 mM NaF, 1 mM Na_3VO_4, 10 µg/ml leupeptin, 10 µg/ml aprotinin, 10 µg/ml pepstatin, and 1 mM phenylmethylsulfonyl fluoride). Protein concentrations were determined using the bicinchoninic acid protein assay kit (Thermo Fisher Scientific). 500 µg of lysate protein was incubated in 1 ml of total volume mRIPA buffer with 2 µg of mouse monoclonal anti-HA, 2 µg of rabbit polyclonal anti-HDAC3, 2 µg of rabbit polyclonal anti-Runx2, (all obtained from Santa Cruz Biotechnology, Inc.), or 2 µg of anti–mouse IgG antibody (Promega) at 4°C. 30 µl of 50% protein A/G–agarose bead slurry (Santa Cruz Biotechnology, Inc.) was added to the lysates and incubated for 2–4 h at 4°C. Beads were washed six to seven times in 1 ml mRIPA. The immune complexes and 30-µg aliquots of total cell lysate of each sample were boiled in 2× SDS-PAGE sample buffer and subjected to immunoblot analysis.

Immunoblot analysis

Samples were resolved by SDS-PAGE and transferred to nitrocellulose membranes (GE Healthcare). Membranes were incubated in TBST buffer (50 mM Tris-HCl, pH 7.5, 150 mM NaCl, and 0.1% Tween 20) with the following primary antibodies: mouse monoclonal anti-Flag antibody (M2; Sigma-Aldrich) 1:5,000 diluted, mouse monoclonal anti-HDAC2 antibody (Sigma-Aldrich) 1:1,000 diluted, mouse monoclonal anti-HA antibody, rabbit polyclonal anti-MTA2 antibody, rabbit polyclonal anti-HDAC3 antibody (all obtained from Santa Cruz Biotechnology, Inc.) 1:500 diluted, mouse monoclonal anti-Xpress antibody (Invitrogen) 1:1,000 diluted, rabbit polyclonal anti-Zfp521 antibody (Wu et al., 2009) 1:500 diluted, or mouse monoclonal antiactin antibody (Millipore) 1:10,000 diluted. Membranes were washed in TBST and incubated with either anti–rabbit or anti–mouse IgG horseradish peroxidase–conjugated secondary antibody (Promega) 1:10,000 diluted for 1 h in TBST. Membranes were washed, incubated for 5 min with the enhanced chemiluminescence system (GE Healthcare), and exposed to film (Kodak).

Zinc removal

Samples were treated as described for immunoprecipitation with the following modification: total cell lysates were incubated in 1 ml mRIPA buffer supplemented with either 50 mM EDTA or 50 mM 1,10-phenanthroline (both purchased from Sigma-Aldrich) with gentle rotation for 2 h at 4°C to chelate the ZF-coordinated zinc ions. Lysates were precleared two times with 30 µl of a 50% slurry of protein A/G–agarose beads followed by immunoprecipitation.

GST pull-down

GST-Zfp521 and GST alone were expressed in DH5-α competent *Escherichia coli* (Invitrogen). Bacterial cultures were incubated with 0.5 mM IPTG (American Bioanalytical) for 3 h to induce recombinant protein expression. Bacteria were lysed in 10 ml of bacterial protein extraction reagent (B-PER; Thermo Fisher Scientific) containing 1 mM NaF, 1 mM Na_3VO_4, 10 µg/ml leupeptin, 10 µg/ml aprotinin, 10 µg/ml pepstatin, and 1 mM phenylmethylsulfonyl fluoride. Lysates were sonicated on ice and cleared by centrifugation. GST alone or GST-Zfp521 was purified by incubating the supernatants with glutathione–Sepharose beads (GE Healthcare) overnight with gentle rotation at 4°C. HEK-293 cells were transfected with 5 µg of plasmid DNA encoding Xpress-tagged Wt Runx2 and Xpress-tagged Runx2 mutants. Transfected cells were lysed, and 500 µg of total cell lysate protein was incubated overnight with 50 µl of a 50% slurry of bead-bound GST or GST-Zfp521 in a total volume of 1 ml mRIPA with gentle agitation at 4°C. Beads were washed four times with mRIPA buffer, boiled in 2× SDS-PAGE sample buffer, and subjected to immunoblot analysis.

DNA affinity precipitation assay

All sense oligonucleotides were biotinylated at the 5′ nucleotide and annealed to their complementary strand. The following oligonucleotides contain a Wt (*wt*, underlined) or mutated (*mu*, lowercase) Runx2 consensus site of the rat Osteocalcin (OG2) promoter: OG2_*wt*_sense, 5′-biotin-CAATCACC<u>AACCACA</u>GCATCCTTTGG-3′, and OG2_*wt*_antisense, 5′-CCAAAGGATGC<u>TGTGGTT</u>GGTGATTG-3′; OG2_*mu*_sense, 5′-biotin-CAATCACCAgtaACAGCATCCTTTGG-3′, and OG2_*mu*_antisense, 5′-CCAAAGGATGCTGTtacTGGTGATTG-3′. In addition, oligonucleotides containing a Wt or mutated Runx2 consensus site of the mouse Osteocalcin (OSE2) promoter were used (Ducy and Karsenty, 1995): OSE2_*wt*_sense, 5′-biotin-GATCCGCTGCAATCACC<u>AACCACA</u>GCA-3′, and OSE2_*wt*_antisense, 5′-GATCTGC<u>TGTGGTT</u>GGTGATTGCAGCG-3′; OSE2_*mu*_sense, 5′-biotin-GATCCGCTGCAATCACCAAgaACAGCA-3′, and OSE2_mu_antisense, 5′-GATCTGCTGTtcTTGGTGATTGCAGCG-3′. Flag-Runx2 was overexpressed in HEK-293 cells alone or together with Flag-Zfp521. Cell lysates were incubated with polydeoxyinosinic-deoxycytidylic acid (Roche) and precleared with streptavidin-agarose (Invitrogen). Pretreated cell lysates were incubated with each oligonucleotide pair and streptavidin-agarose. The protein–DNA–streptavidin–agarose complex was separated using an SDS-PAGE. Flag-Runx2 was detected on immunoblots using an anti-Flag antibody (M2).

Quantitative RT-PCR analysis

The mid-diaphysis of the femora was ground in liquid nitrogen followed by an RNA extraction using TRIZOL reagent (Invitrogen) and an RNA cleanup using the RNeasy Mini kit (QIAGEN) according to the manufacturer's protocols. RNA from cells was isolated using the RNeasy Mini kit, including an on-column RNase-free DNase 1 digestion according to the manufacturer's instructions. RNA was quantified spectrophotometrically. cDNA was synthesized by reverse transcription. 1 µg of total RNA was mixed with 3 µl of an oligonucleotide combination of 0.25 µg/µl oligo-$dT_{12–18}$ and 0.25 µg/µl of random primers (both obtained from Invitrogen) in a 3:1 ratio. The volume was adjusted to 20 µl with water, and the mixture was incubated for 10 min at 70°C. Reverse transcription was performed in 40 µl of total volume after addition of 17 µl of reaction mix containing 8 µl of 5× first strand buffer, 4 µl of 5-mmol/µl deoxynucleoside triphosphate, 4 µl of 0.1-M DTT, and 1 µl of 200-U/µl SuperScript 2 (all purchased from Invitrogen). Incubation was performed at 42°C for 50 min followed by an incubation at 70°C for 10 min. Volumes were adjusted to 100 µl by adding 60 µl of water. 1 µl cDNA was mixed with 12.5 µl of green supermix (iQ SYBR; Bio-Rad Laboratories), 10.5 µl of water, and 0.5 µl of 10-µM sense and antisense oligonucleotides. The following oligonucleotides were used for gene expression analyses: glyceraldehyde 3-phosphate dehydrogenase, 5′-GGTCGGTGTGAACGGATTTGGC-3′ and 5′-GCAGTGATGGCATGGACTGTGG-3′; Runx2, 5′-TCCACAAGGACAGAGTCAGATTACAG-3′ and 5′-CAGAAGTCAGAGGTGGCAGTGTCATC-3′; Osx, 5′-TCTGCTTGAGGAAGAAGCTCACTATGGC-3′ and 5′-AGGCAGTCAGACGAGCTGTGC-3′; Dmp-1, 5′-CCAGAGGGACAGGCAAATAG-3′ and 5′-CTGGACTGTGTGGTGTCTGC-3′; Zfp521, 5′-CAACGAGTGGGACATCCAGGTTC-3′ and 5′-CATCGTATGATTCTGTAGCTCTGTTTGG-3′; Rankl, 5′-CAAGCTCCGAGCTGGTGAAG-3′ and 5′-CCTGAACTTTGAAAGCCCCA-3′; and Opg, 5′-AAGAGCAAACCTTCCAGCTGC-3′ and 5′-CACGCTGCTTTCACAGAGGTC-3′. The reactions were performed in a 96-well plate using an iCycler (Bio-Rad Laboratories). Samples were denatured at 95°C for 3 min. cDNA was amplified by 40 cycles at 95, 57, and 72°C for 30 s each. All samples were normalized to glyceraldehyde 3-phosphate dehydrogenase, and relative expression of Zfp521 was determined using the $2^{-\Delta\Delta CT}$ method. Data are presented as fold change relative to control samples.

Luciferase reporter gene assay

Cells were plated at a density of 2×10^5 cells per well in 6-well tissue culture plates and grown in α-MEM until 70–80% confluency. Cells were transfected with the 6×OSE2-luc reporter plasmid together with the following plasmids as indicated: 1 µg Flag-Runx2, 2 µg HA-Zfp521, 2 µg HA-mu_Zfp521, 1 µg Flag-HDAC3, and 1 µg each pSHAG-HDAC3 shRNA and scrambled control. 17 ng pCMV-Renilla-luciferase (Promega) was used for normalization. In all transfection assays, empty vector DNA was used to equalize the total amount of DNA. After 24 h, 100 nM TSA (Sigma-Aldrich) was added. Luciferase activity was determined 48 h after transfection using the dual-luciferase reporter assay kit (Promega) as described by the manufacturer.

Osteoblast differentiation assay

Cells were washed twice with PBS and fixed for 10 min in 3.7% formaldehyde. To stain for ALP activity, cells were incubated with staining mix (35 mg Fast blue RR Salt [Sigma-Aldrich] dissolved in 2 ml naphthol AS-BI alkaline solution [Sigma-Aldrich] in 48 ml of deionized water) for 30 min in the

dark. Images of stained cells were obtained using a scanner (Scanjet 5530) and imaging software (Photosmart Studio; Hewlett-Packard). ALP activity in total cell lysate was quantified using an ALP kit (LabAssay; Wako Chemicals USA, Inc.) according to the manufacturer's instructions.

Animals

The *ENO2-tTA* mice (Chen et al., 1998), *TetOp-Zfp521* mice (Wu et al., 2009), *Runx2*$^{+/-}$ mice (provided by B. Olsen, Harvard School of Dental Medicine, Boston, MA; Otto et al., 1997), and *Col1-2.3kb–Runx2* mice (referred to as *Runx2*^{Tg} mice) were described previously (Geoffroy et al., 2002). *Zfp521*$^{+/-}$ mice were generated using standard recombineering techniques and provided by S. Warming (Genentech, South San Francisco, CA). Animals were genotyped by standard PCR (95°C for 15 s, 60°C for 30 s, and 72°C for 30 s for 35 cycles) using the following oligonucleotides: Zfp521_*Wt*_sense, 5′-GCTCCTTCACATGCTCACA-3′; Zfp521_*Wt*_antisense, 5′-CTGGCATGGGTAAGGCAGT-3′; and Zfp521_*Ko*_antisense, 5′-CTCCGAGAGTTTGAGTGCAA-3′. The following fragments were obtained: 502-bp $^{+/+}$ band (*Wt* sense + *Wt* antisense), 382-bp$^{-/-}$ band (*Wt* sense + *Ko* antisense), and 502-bp + 382-bp$^{+/-}$ band (*Wt* sense + *Wt* antisense + *Ko* antisense). *Zfp521*$^{+/-}$ mice were mated with *Runx2*$^{+/-}$ mice to obtain *Zfp521*$^{+/+}$*;Runx2*$^{+/+}$, *Zfp521*$^{+/-}$*;Runx2*$^{+/+}$, *Zfp521*$^{+/+}$*;Runx2*$^{+/-}$, and *Zfp521*$^{+/-}$*;Runx2*$^{+/-}$ mice. *Runx2*$^{+/-}$ and *Runx2*^{Tg} mice were mated with *TetOp-Zfp521* mice. F1 mice with the genotype *Runx2*$^{+/-}$*;TetOp-Zfp521* or *Runx2-TG;TetOp-Zfp521* were crossed with mice homozygous for *ENO2-tTA*. All offsprings of the F2 generation carried one *ENO2-tTA* transgene and had one of the following genotypes: *Runx2*$^{+/+}$*;TetOp-Zfp521-Wt*, *Runx2*$^{+/+}$*;TetOp-Zfp521*^{Tg}, *Runx2*$^{+/-}$*;TetOp-Zfp521-Wt*, *Runx2*$^{+/-}$*;TetOp-Zfp521*^{Tg}, *Runx2-Wt;Zfp521-Wt*, *Runx2-Wt;Zfp521*^{Tg}, *Runx2*^{Tg}*;Zfp521-Wt*, or *Runx2*^{Tg}*;Zfp521*^{Tg}. These mating strategies provided all experimental mice as well as all controls. Mice from all crosses appeared at the expected Mendelian ratio. Littermates were used for analysis.

Isolation of primary osteoblasts

Calvariae were dissected from 1–3-d-old neonatal mice and sequentially digested for 15 min in α-MEM containing 0.1% collagenase and 0.2% dispase (both purchased from Roche). Cells obtained from fractions 2–3 were combined according to the genotype and expanded in α-MEM containing 10% FBS, 100 U/ml penicillin, and 100 µg/ml streptomycin.

Colony-forming unit assays

Colony-forming unit assays (CFU-F and CFU-OB) were performed using bone marrow cells from *Zfp521*^{Tg} mice and control littermates. Cells were obtained by flushing the marrow cavity of the femur with α-MEM containing 10% FBS, 100 U/ml penicillin, and 100 µg/ml streptomycin using a 23-gauge needle. Cells were homogenized by gentle pipetting and counted using a hemocytometer. Nucleated cells were seeded at a density of 1.5×10^6 cells per well in a 6-well dish and maintained under osteogenic culture conditions. To determine CFU-F, cells were stained for ALP after 10 d in culture. Cell colonies containing at least 20 cells were designated CFU-F. For the determination of CFU-OB, cells were maintained for 20 d and then stained for mineralization using the von Kossa stain. Mineralized nodules were designated CFU-OB.

Proliferation assay

Calvarial osteoblasts from *Zfp521*^{Tg} mice and *Wt* littermates were plated in triplicate at a density of 10^5 cells per well in a 6-well plate. On the next day, cells were incubated with 1 µCi [^{3}H]thymidine per well for 4 h at 37°C. Cells were dissolved in 1% SDS, and [^{3}H]thymidine incorporation was determined using a scintillation counter (LS 6500; Beckmann Coulter).

Immunocytochemistry

Calvarial osteoblasts from *Zfp521*^{Tg} mice and *Wt* littermates were cultured on glass coverslips in osteogenic medium for 5 d. Cells were fixed in 3.7% formaldehyde and immunostained with rabbit polyclonal anti-Runx2 antibody at a 1:100 dilution and Alexa Fluor fluorescent conjugated secondary antibody (Invitrogen). ToPro (Invitrogen) was used at a 1:1,000 dilution for nuclear labeling. Slides were mounted using FluorSave (EMD). Images were obtained at room temperature using a laser-scanning microscope (LSM 510 Meta; Carl Zeiss, Inc.) equipped with a Plan Neofluar 63×/1.4 NA water immersion lens and LSM 510 software. To prevent interference between fluorochromes, each channel was imaged sequentially using the multitrack recording module before merging. Total enhancements were performed using Photoshop (CS2; Adobe).

Skeletal analyses

Offspring of the *Zfp521*^{Tg} × *Runx2*^{Tg} cross were injected 7 and 2 d before sacrifice with calcein (40 mg/kg of body weight) and democycline (20 mg/kg of body weight; both obtained from Sigma-Aldrich), respectively. Tibiae of 5-wk-old female mice were collected and fixed in 3.7% PBS-buffered formaldehyde. For histomorphometrical analysis, tibiae were embedded in methylmethacrylate, and Toluidine blue and von Kossa stainings were performed using 5-µm sagittal sections. Quantitative bone histomorphotric measurements were performed according to standardized protocols (Parfitt et al., 1987) using the OsteoMeasure system (OsteoMetrics). Cortical porosity was determined after staining with Sirius red. Tartrate-resistant acid phosphatase staining was performed after decalcification and paraffin embedding. All histological images were obtained at room temperature using a microscope (Eclipse E800; Nikon) with a 20× (no medium; NA 0.50) objective fitted with a camera (DP71) and software (DP controller; Olympus). Plain radiographs were taken (29 kV for 10 s) using an x-ray apparatus (Micro 50; Micro Focus Imaging). Films were scanned (Scanjet 5530) and saved (Photosmart Studio software). For whole-mount skeletal preparations, skins were removed, and mice were eviscerated. Samples were stained with Alcian blue/Alizarin red solution (644 ml of 95% ethanol/liter, 131 ml acetic acid/liter, 47 mg Alcian blue/liter, and 20 mg Alizarin red/liter) for 5 d followed by digestion using 1.8% KOH until the soft tissue was cleared. Samples were preserved in 50% glycerol. Skeletal elements remained in glycerol, and images were taken at room temperature using a microscope (Stereo Discovery V8; Carl Zeiss, Inc.) with a Plan S 1.25–1.6× FWD 81-mm objective equipped with a camera (Axiocam HRC REV.2; Carl Zeiss, Inc.) and basic software (AV4; Carl Zeiss, Inc.). The length of the mineralized clavicle and the hyoid bone was measured by drawing a scale bar along the mineralized tissue using the microscope image software. To quantify the fontanelle area, three coronal diameters (rostral, central, and caudal) were measured, and the mean coronal diameter was determined. The mean of the coronal diameter and the sagittal diameter were then used to calculate the approximate fontanelle area.

In situ hybridization

[^{35}S]UTP-labeled riboprobes to detect transcripts encoding Osteocalcin, Osteopontin, and Dmp-1 (all provided by B. Lanske, Harvard School of Dental Medicine, Boston, MA) were synthesized from linearized plasmids using an in vitro transcription kit (Promega) and [^{35}S]UTP (GE Healthcare). In situ hybridization was performed on decalcified and paraffin-embedded proximal tibiae. After removing paraffin by xylene, samples were rehydrated using an ethanol series. Sections were treated with proteinase K and 4% paraformaldehyde followed by incubation with 0.2 N HCl. 0.25% acetic anhydride in triethanolamine buffer was used for acetylation. Before hybridization, sections were dehydrated in ethanol and air dried. Sections were then hybridized with ^{35}S-labeled sense riboprobes in a humidified chamber at 50°C for 16 h. Sections were washed with 2× SSC and 2× SSC/50% formamide at 50°C and treated with RNase at 37°C for 20 min. After dehydration sections were air dried and coated with emulsion (NTB2, 1:1 dilution with water; Kodak), they were developed with developer (Dektol) and fixed with fixer (Kodak). Before analysis, sections were counterstained with hematoxylin and eosin. Osteocytes were counted per bone volume in the cortex of the mid-diaphysis. Images were taken at room temperature using a microscope (Eclipse E800) with a 20× (no medium; NA 0.50) objective and a camera (DP71) with DP controller software.

Microcomputed tomography

3D vertebral body trabecular bone properties were analyzed. The fifth lumbar vertebral bodies (L5) of four *Wt* mice and nine *Zfp521*^{Tg} mice were analyzed using high-resolution microcomputed tomography with a fixed isotropic voxel size of 10.5 µm (70 peak kV at 114 µA; Viva40 micro-CT; Scanco Medical AG). The cortical bone was manually excluded from the analysis. A fixed global threshold of 190 mg HA/cm^3 was selected, which allowed the rendering of mineralized tissue only. This threshold was verified by manually evaluating 10 single tomographic slices from four samples per group to isolate the mineralized tissue and to preserve its morphology while excluding nonmineralized tissues. All analyses were performed on the digitally extracted bone tissue using 3D distance techniques (Scanco Medical AG).

Statistics

Mean values and the SEM were calculated. To determine significant differences, the means of all groups were first analyzed by analysis of variance. If an F test yielded significant results ($P < 0.05$), groups were compared

using Fisher's protected least significant difference posthoc test. Calculations were performed using the StatView 4.1 statistic analysis software (Statistical Analysis System Institute). P-values <0.05 were considered significant.

Online supplemental material

Fig. S1 shows the expression of Zfp521 in osteoblasts of neonatal *Zfp521*^{Tg} mice, the dose-dependent antagonism of Runx2 activity by Zfp521, and the Zfp521-mediated repression of the Runx2-induced early osteoblast differentiation. Fig. S2 demonstrates the interaction between HA-Zfp521 and Flag-Runx2 and the reduced interaction of HA-tagged mutated Zfp521 with Flag-Runx2. Fig. S3 displays the disabled interaction of HA-Δ13Zfp521 with components of the NuRD complex, the efficiency of shHDAC3, and the interaction of HA-Zfp521 with Flag-HDAC3. Fig. S4 shows the concurrent expression of the Zfp521 and the Runx2 transgenes in the long bones of adult *Zfp521*^{Tg} and *Runx2*^{Tg} mice, respectively. Fig. S5 demonstrates the high bone mass in the lumbar spine of *Zfp521*^{Tg} mice. Online supplemental material is available at http://www.jcb.org/cgi/content/full/jcb.201009107/DC1.

We thank Rik Derynck for ROS17/2.8 and ROS-H14 cells; Jennifer Westendorf for the expression vectors Flag-HDAC3, pSHAG-HDAC3 shRNA, and scrambled control; Patricia Ducy for the Flag-Runx2 and the 6×OSE2-luc constructs; Björn Olsen for *Runx2*$^{+/-}$ mice; and Beate Lanske for providing riboprobes and for helpful discussions. We are grateful to Despina Sitara for help with the in situ hybridizations and thank Karen Cox for expert help with imaging studies. We are indebted to Giovanni Morrone for fruitful scientific conversations.

Support was provided in part by the National Institutes of Health National Institute of Arthritis and Musculoskeletal and Skin Diseases grants AR048218 and AR057769 (R. Baron). Additional support was provided by the Deutsche Forschungsgemeinschaft grant HE 5208/1-1 (E. Hesse), the Gideon and Sevgi Rodan Fellowship from the International Bone and Mineral Society (E. Hesse and R. Kiviranta), the Academy of Finland (R. Kiviranta), the Harvard School of Dental Medicine Dean's Scholars Award (E. Hesse), the National Institutes of Health training grant GM07527 (D. Correa), and the George Robert Pfeiffer Fellowship from the Gustavus and Louise Pfeiffer Research Foundation (D. Correa).

Submitted: 22 September 2010
Accepted: 17 November 2010

References

Bialek, P., B. Kern, X. Yang, M. Schrock, D. Sosic, N. Hong, H. Wu, K. Yu, D.M. Ornitz, E.N. Olson, et al. 2004. A twist code determines the onset of osteoblast differentiation. *Dev. Cell.* 6:423–435. doi:10.1016/S1534-5807(04)00058-9

Bond, H.M., M. Mesuraca, E. Carbone, P. Bonelli, V. Agosti, N. Amodio, G. De Rosa, M. Di Nicola, A.M. Gianni, M.A.S. Moore, et al. 2004. Early hematopoietic zinc finger protein (EHZF), the human homolog to mouse Evi3, is highly expressed in primitive human hematopoietic cells. *Blood.* 103:2062–2070. doi:10.1182/blood-2003-07-2388

Bond, H.M., M. Mesuraca, N. Amodio, T. Mega, V. Agosti, D. Fanello, D. Pelaggi, L. Bullinger, M. Grieco, M.A. Moore, et al. 2008. Early hematopoietic zinc finger protein-zinc finger protein 521: a candidate regulator of diverse immature cells. *Int. J. Biochem. Cell Biol.* 40:848–854. doi:10.1016/j.biocel.2007.04.006

Chen, J., M.B. Kelz, G. Zeng, N. Sakai, C. Steffen, P.E. Shockett, M.R. Picciotto, R.S. Duman, and E.J. Nestler. 1998. Transgenic animals with inducible, targeted gene expression in brain. *Mol. Pharmacol.* 54:495–503.

Compston, J.E. 2007. Skeletal actions of intermittent parathyroid hormone: effects on bone remodelling and structure. *Bone.* 40:1447–1452. doi:10.1016/j.bone.2006.09.008

Correa, D., E. Hesse, D. Seriwatanachai, R. Kiviranta, H. Saito, K. Yamana, L. Neff, A. Atfi, L. Coillard, D. Sitara, et al. 2010. Zfp521 is a target gene and key effector of parathyroid hormone-related peptide signaling in growth plate chondrocytes. *Dev. Cell.* 19:533–546. doi:10.1016/j.devcel.2010.09.008

de Frutos, C.A., R. Dacquin, S. Vega, P. Jurdic, I. Machuca-Gayet, and M.A. Nieto. 2009. Snail1 controls bone mass by regulating Runx2 and VDR expression during osteoblast differentiation. *EMBO J.* 28:686–696. doi:10.1038/emboj.2009.23

Derynck, R., and R.J. Akhurst. 2007. Differentiation plasticity regulated by TGF-beta family proteins in development and disease. *Nat. Cell Biol.* 9:1000–1004. doi:10.1038/ncb434

Drissi, H., Q. Luc, R. Shakoori, S. Chuva De Sousa Lopes, J.Y. Choi, A. Terry, M. Hu, S. Jones, J.C. Neil, J.B. Lian, et al. 2000. Transcriptional autoregulation of the bone related CBFA1/RUNX2 gene. *J. Cell. Physiol.* 184:341–350. doi:10.1002/1097-4652(200009)184:3<341::AID-JCP8>3.0.CO;2-Z

Ducy, P., and G. Karsenty. 1995. Two distinct osteoblast-specific cis-acting elements control expression of a mouse osteocalcin gene. *Mol. Cell. Biol.* 15:1858–1869.

Ducy, P., R. Zhang, V. Geoffroy, A.L. Ridall, and G. Karsenty. 1997. Osf2/Cbfa1: a transcriptional activator of osteoblast differentiation. *Cell.* 89:747–754. doi:10.1016/S0092-8674(00)80257-3

Galindo, M., J. Pratap, D.W. Young, H. Hovhannisyan, H.J. Im, J.Y. Choi, J.B. Lian, J.L. Stein, G.S. Stein, and A.J. van Wijnen. 2005. The bone-specific expression of Runx2 oscillates during the cell cycle to support a G1-related antiproliferative function in osteoblasts. *J. Biol. Chem.* 280:20274–20285. doi:10.1074/jbc.M413665200

Geoffroy, V., M. Kneissel, B. Fournier, A. Boyde, and P. Matthias. 2002. High bone resorption in adult aging transgenic mice overexpressing cbfa1/runx2 in cells of the osteoblastic lineage. *Mol. Cell. Biol.* 22:6222–6233. doi:10.1128/MCB.22.17.6222-6233.2002

Giner, M., M.J. Montoya, M.A. Vázquez, M.J. Rios, R. Moruno, M.J. Miranda, and R. Pérez-Cano. 2008. Modifying RANKL/OPG mRNA expression in differentiating and growing human primary osteoblasts. *Horm. Metab. Res.* 40:869–874. doi:10.1055/s-0028-1082083

Harada, S., and G.A. Rodan. 2003. Control of osteoblast function and regulation of bone mass. *Nature.* 423:349–355. doi:10.1038/nature01660

Hartmann, C. 2009. Transcriptional networks controlling skeletal development. *Curr. Opin. Genet. Dev.* 19:437–443. doi:10.1016/j.gde.2009.09.001

Hassan, M.Q., A. Javed, M.I. Morasso, J. Karlin, M. Montecino, A.J. van Wijnen, G.S. Stein, J.L. Stein, and J.B. Lian. 2004. Dlx3 transcriptional regulation of osteoblast differentiation: temporal recruitment of Msx2, Dlx3, and Dlx5 homeodomain proteins to chromatin of the osteocalcin gene. *Mol. Cell. Biol.* 24:9248–9261. doi:10.1128/MCB.24.20.9248-9261.2004

Hassan, M.Q., S. Saini, J.A. Gordon, A.J. van Wijnen, M. Montecino, J.L. Stein, G.S. Stein, and J.B. Lian. 2009. Molecular switches involving homeodomain proteins, HOXA10 and RUNX2 regulate osteoblastogenesis. *Cells Tissues Organs.* 189:122–125. doi:10.1159/000151453

Hesslein, D.G., J.A. Fretz, Y. Xi, T. Nelson, S. Zhou, J.A. Lorenzo, D.G. Schatz, and M.C. Horowitz. 2009. Ebf1-dependent control of the osteoblast and adipocyte lineages. *Bone.* 44:537–546. doi:10.1016/j.bone.2008.11.021

Jensen, E.D., T.M. Schroeder, J. Bailey, R. Gopalakrishnan, and J.J. Westendorf. 2008. Histone deacetylase 7 associates with Runx2 and represses its activity during osteoblast maturation in a deacetylation-independent manner. *J. Bone Miner. Res.* 23:361–372. doi:10.1359/jbmr.071104

Jensen, E.D., R. Gopalakrishnan, and J.J. Westendorf. 2009. Bone morphogenic protein 2 activates protein kinase D to regulate histone deacetylase 7 localization and repression of Runx2. *J. Biol. Chem.* 284:2225–2234. doi:10.1074/jbc.M800586200

Kang, J.S., T. Alliston, R. Delston, and R. Derynck. 2005. Repression of Runx2 function by TGF-beta through recruitment of class II histone deacetylases by Smad3. *EMBO J.* 24:2543–2555. doi:10.1038/sj.emboj.7600729

Karsenty, G., H.M. Kronenberg, and C. Settembre. 2009. Genetic control of bone formation. *Annu. Rev. Cell Dev. Biol.* 25:629–648. doi:10.1146/annurev.cellbio.042308.113308

Kolf, C.M., E. Cho, and R.S. Tuan. 2007. Mesenchymal stromal cells. Biology of adult mesenchymal stem cells: regulation of niche, self-renewal and differentiation. *Arthritis Res. Ther.* 9:204. doi:10.1186/ar2116

Komori, T., H. Yagi, S. Nomura, A. Yamaguchi, K. Sasaki, K. Deguchi, Y. Shimizu, R.T. Bronson, Y.-H. Gao, M. Inada, et al. 1997. Targeted disruption of *Cbfa1* results in a complete lack of bone formation owing to maturational arrest of osteoblasts. *Cell.* 89:755–764. doi:10.1016/S0092-8674(00)80258-5

Li, X., P. Liu, W. Liu, P. Maye, J. Zhang, Y. Zhang, M. Hurley, C. Guo, A. Boskey, L. Sun, et al. 2005. Dkk2 has a role in terminal osteoblast differentiation and mineralized matrix formation. *Nat. Genet.* 37:945–952. doi:10.1038/ng1614

Lian, J.B., and G.S. Stein. 2003. Runx2/Cbfa1: a multifunctional regulator of bone formation. *Curr. Pharm. Des.* 9:2677–2685. doi:10.2174/1381612033453659

Lian, J.B., G.S. Stein, A. Javed, A.J. van Wijnen, J.L. Stein, M. Montecino, M.Q. Hassan, T. Gaur, C.J. Lengner, and D.W. Young. 2006. Networks and hubs for the transcriptional control of osteoblastogenesis. *Rev. Endocr. Metab. Disord.* 7:1–16. doi:10.1007/s11154-006-9001-5

Liu, W., S. Toyosawa, T. Furuichi, N. Kanatani, C. Yoshida, Y. Liu, M. Himeno, S. Narai, A. Yamaguchi, and T. Komori. 2001. Overexpression of Cbfa1 in osteoblasts inhibits osteoblast maturation and causes osteopenia with multiple fractures. *J. Cell Biol.* 155:157–166. doi:10.1083/jcb.200105052

Lou, Y., A. Javed, S. Hussain, J. Colby, D. Frederick, J. Pratap, R. Xie, T. Gaur, A.J. van Wijnen, S.N. Jones, et al. 2009. A Runx2 threshold for

the cleidocranial dysplasia phenotype. *Hum. Mol. Genet.* 18:556–568. doi:10.1093/hmg/ddn383

Moore, K.A., and I.R. Lemischka. 2006. Stem cells and their niches. *Science.* 311:1880–1885. doi:10.1126/science.1110542

Mundlos, S., F. Otto, C. Mundlos, J.B. Mulliken, A.S. Aylsworth, S. Albright, D. Lindhout, W.G. Cole, W. Henn, J.H. Knoll, et al. 1997. Mutations involving the transcription factor CBFA1 cause cleidocranial dysplasia. *Cell.* 89:773–779. doi:10.1016/S0092-8674(00)80260-3

Nakashima, K., X. Zhou, G. Kunkel, Z. Zhang, J.M. Deng, R.R. Behringer, and B. de Crombrugghe. 2002. The novel zinc finger-containing transcription factor osterix is required for osteoblast differentiation and bone formation. *Cell.* 108:17–29. doi:10.1016/S0092-8674(01)00622-5

Otto, F., A.P. Thornell, T. Crompton, A. Denzel, K.C. Gilmour, I.R. Rosewell, G.W. Stamp, R.S. Beddington, S. Mundlos, B.R. Olsen, et al. 1997. Cbfa1, a candidate gene for cleidocranial dysplasia syndrome, is essential for osteoblast differentiation and bone development. *Cell.* 89:765–771. doi:10.1016/S0092-8674(00)80259-7

Otto, F., H. Kanegane, and S. Mundlos. 2002. Mutations in the RUNX2 gene in patients with cleidocranial dysplasia. *Hum. Mutat.* 19:209–216. doi:10.1002/humu.10043

Parfitt, A.M., M.K. Drezner, F.H. Glorieux, J.A. Kanis, H. Malluche, P.J. Meunier, S.M. Ott, and R.R. Recker. 1987. Bone histomorphometry: standardization of nomenclature, symbols, and units. Report of the ASBMR Histomorphometry Nomenclature Committee. *J. Bone Miner. Res.* 2:595–610. doi:10.1002/jbmr.5650020617

Razidlo, D.F., T.J. Whitney, M.E. Casper, M.E. McGee-Lawrence, B.A. Stensgard, X. Li, F.J. Secreto, S.K. Knutson, S.W. Hiebert, and J.J. Westendorf. 2010. Histone deacetylase 3 depletion in osteo/chondroprogenitor cells decreases bone density and increases marrow fat. *PLoS One.* 5:e11492. doi:10.1371/journal.pone.0011492

Rodda, S.J., and A.P. McMahon. 2006. Distinct roles for Hedgehog and canonical Wnt signaling in specification, differentiation and maintenance of osteoblast progenitors. *Development.* 133:3231–3244. doi:10.1242/dev.02480

Rowe, G.C., C.S. Choi, L. Neff, W.C. Horne, G.I. Shulman, and R. Baron. 2009. Increased energy expenditure and insulin sensitivity in the high bone mass DeltaFosB transgenic mice. *Endocrinology.* 150:135–143. doi:10.1210/en.2008-0678

Sabatakos, G., N.A. Sims, J. Chen, K. Aoki, M.B. Kelz, M. Amling, Y. Bouali, K. Mukhopadhyay, K. Ford, E.J. Nestler, and R. Baron. 2000. Overexpression of DeltaFosB transcription factor(s) increases bone formation and inhibits adipogenesis. *Nat. Med.* 6:985–990. doi:10.1038/79683

Sabatakos, G., G.C. Rowe, M. Kveiborg, M. Wu, L. Neff, R. Chiusaroli, W.M. Philbrick, and R. Baron. 2008. Doubly truncated FosB isoform (Delta2DeltaFosB) induces osteosclerosis in transgenic mice and modulates expression and phosphorylation of Smads in osteoblasts independent of intrinsic AP-1 activity. *J. Bone Miner. Res.* 23:584–595. doi:10.1359/jbmr.080110

Schroeder, T.M., R.A. Kahler, X. Li, and J.J. Westendorf. 2004. Histone deacetylase 3 interacts with runx2 to repress the osteocalcin promoter and regulate osteoblast differentiation. *J. Biol. Chem.* 279:41998–42007. doi:10.1074/jbc.M403702200

Stein, G.S., J.B. Lian, A.J. van Wijnen, J.L. Stein, M. Montecino, A. Javed, S.K. Zaidi, D.W. Young, J.-Y. Choi, and S.M. Pockwinse. 2004. Runx2 control of organization, assembly and activity of the regulatory machinery for skeletal gene expression. *Oncogene.* 23:4315–4329. doi:10.1038/sj.onc.1207676

Turner, J., and M. Crossley. 1999. Mammalian Krüppel-like transcription factors: more than just a pretty finger. *Trends Biochem. Sci.* 24:236–240. doi:10.1016/S0968-0004(99)01406-1

van der Horst, G., S.M. van der Werf, H. Farih-Sips, R.L. van Bezooijen, C.W. Löwik, and M. Karperien. 2005. Downregulation of Wnt signaling by increased expression of Dickkopf-1 and -2 is a prerequisite for late-stage osteoblast differentiation of KS483 cells. *J. Bone Miner. Res.* 20:1867–1877. doi:10.1359/JBMR.050614

Westendorf, J.J., S.K. Zaidi, J.E. Cascino, R. Kahler, A.J. van Wijnen, J.B. Lian, M. Yoshida, G.S. Stein, and X. Li. 2002. Runx2 (Cbfa1, AML-3) interacts with histone deacetylase 6 and represses the p21(CIP1/WAF1) promoter. *Mol. Cell. Biol.* 22:7982–7992. doi:10.1128/MCB.22.22.7982-7992.2002

Wu, M., E. Hesse, F. Morvan, J.P. Zhang, D. Correa, G.C. Rowe, R. Kiviranta, L. Neff, W.M. Philbrick, W.C. Horne, and R. Baron. 2009. Zfp521 antagonizes Runx2, delays osteoblast differentiation in vitro, and promotes bone formation in vivo. *Bone.* 44:528–536. doi:10.1016/j.bone.2008.11.011